Biomarkers in the rock outcrop of the Kazusa Group reveal paleoenvironments of the Kuroshio region

HIROTO KAJITA (kajita@aori.u-tokyo.ac.jp)
The University of Tokyo https://orcid.org/0000-0003-0399-6483

Ayumi Maeda
The University of Tokyo

Masayuki Utsunomiya
National Institute of Advanced Industrial Science and Technology

Toshihiro Yoshimura
Japan Agency for Marine-Earth Science and Technology https://orcid.org/0000-0003-0478-4239

Naohiko Ohkouchi
Japan Agency for Marine-Earth Science and Technology

Atsushi Suzuki
National Institute of Advanced Industrial Science and Technology

Hodaka Kawahata
The University of Tokyo

Article

Keywords: long-chain alkenones, n-alkanes, biomarkers, oceanic and atmospheric changes

Posted Date: September 28th, 2020

DOI: https://doi.org/10.21203/rs.3.rs-72985/v1

Version of Record: A version of this preprint was published at Communications Earth & Environment on May 10th, 2021. See the published version at https://doi.org/10.1038/s43247-021-00154-2.

Biomarkers in the rock outcrop of the Kazusa Group reveal paleoenvironments of the Kuroshio region

Hiroto Kajita[1,2,3,4,*], Ayumi Maeda[1,2,3,4], Masayuki Utsunomiya[3], Toshihiro Yoshimura[4], Naohiko Ohkouchi[4], Atsushi Suzuki[3], Hodaka Kawahata[1,2]

[1] *Atmosphere and Ocean Research Institute, University of Tokyo, 5-1-5, Japan*

[2] *Department of Earth and Planetary Science, Graduate School of Science, University of Tokyo, Japan*

[3] *Geological Survey of Japan, National Institute of Advanced Industrial Science and Technology, Japan*

[4] *Biogeochemistry Research Center, Japan Agency for Marine-Earth Science and Technology, Japan*

* Correspondence: H.K., Email: kajita322@frontier.hokudai.ac.jp, Tel: (+81) 04 7136 6135

Abstract

The classical biomarkers of long-chain alkenones and *n*-alkanes preserved in marine and lake sediment cores are widely used to reconstruct paleoenvironments. Here, we detected these biomarkers are preserved in the rock outcrop of the Kazusa Group exposed in central Japan, the most continuous sedimentary succession in the world, covering almost the entire Pleistocene. The alkenone unsaturation ratio and average chain length of *n*-alkanes appeared to reflect the glacial-interglacial changes in the sea surface temperature (SST) and terrestrial climate, respectively. Alkenone-based SSTs during 1.1–1.0 Ma were significantly higher than present-day SSTs in the same area, as supported by foraminiferal Mg/Ca-based temperatures, possibly reflecting the direct intrusion of the warm Kuroshio Current. Applying these biomarkers, which might be circumstantially preserved owing to their immunity to high temperature and consolidation stress during burial and uplift, we expect that the Kazusa Group should reveal detailed oceanic and atmospheric changes of the Kuroshio region.

Introduction

Long-chain alkenones (LCAs) are C_{35}–C_{42} unsaturated methyl and ethyl ketones with 2–4 double bonds and feature unique lipid biomarkers produced by Isochrysidales haptophytes living in surface waters[1]. The degree of unsaturation in C_{37} alkenones ($U^{K'}_{37}$) is strongly correlated with the growth temperature in culture experiments, and is widely used as one of the most quantitative and well-established proxies for sea surface temperature (SST)[2–4]. High-molecular (> C_{27}) *n*-alkanes with odd/even predominance are derived from terrestrial higher plants[5,6] and are used to reconstruct changes in the temperature, humidity, and vegetation based on the carbon number distributions[7,8]. These paleoenvironmental indexes are traditionally applied to marine and lake sediment cores, but are rarely applied to exposed sedimentary rocks because LCAs and *n*-alkanes can undergo maturation at high temperature and lose their initial paleoenvironmental information[9,10]. Several previous studies have detected LCAs and *n*-alkanes from outcrops; however, only a few studies conducted on the outcrops around the Mediterranean Sea, reproduced distinct glacial-interglacial-scale climate changes using $U^{K'}_{37}$, and there are no studies in which *n*-alkane-based indexes were used[7,11,12].

The Kazusa Group represents the infill of the Plio-Pleistocene Kazusa forearc basin that developed in response to the subduction of the Pacific and Philippine Sea plates beneath the North American plate, and is well exposed in the Boso Peninsula, Chiba Prefecture, central Japan[13] (Fig. 1). The middle to lower part of the Kazusa Group is represented by successions of submarine fan deposits associated with deep-sea, basin-plain, and slope deposits, and is one of the most continuous of exposed sedimentary successions with a high sedimentation rate (ca. 1.5 m/kyr on average) in the world covering almost the entire Pleistocene[13,14]. It contains marine microfossils, paleomagnetic reversals, and a large number of tephra beds, which allow us to

establish a robust chronological and stratigraphic framework and undertake paleoceanographic and paleoclimatic studies with high time-resolution[15] (Supplementary Fig. 1). These studies are recognised worldwide, and the Chiba composite section in the Kazusa Group was certified in 2020 as the Global Boundary Stratotype Section and Point (GSSP) between the Chibanian and Calabrian stages[16].

The Boso Peninsula is located near the Kuroshio Extension Front (KEF), where the Kuroshio Current (KC) leaves the coast of Japan. The KC transports warm and saline water from the equatorial Western Pacific Warm Pool (WPWP) to northern mid-latitudes, and forms pronounced latitudinal gradients in SST off the Boso Peninsula[17] (Supplementary Fig. 2). It is also located at the northern limit of the seasonal progression of the westerly jet that bounds the East Asian monsoon (EAM) front[18]. Thus, the oceanic and terrestrial conditions around the Kazusa forearc basin should be responsive to shifts in the KEF and EAM, which are related to the modulations in the dynamics of Hadley cells in the northern hemisphere[17,18]. Therefore, the paleoenvironmental information, especially SST, stored in the Kazusa Group could be important for understanding the changes in global climate systems during the Pleistocene. However, there has been no widely applicable quantitative proxy for SST owing to the extremely small standing stock and poor preservation of surface-dwelling planktic foraminifera. In this study, we discovered that multiple classical biomarkers, LCAs and odd preference *n*-alkanes, are well preserved in several sections of the Kazusa Group and can be used as paleoenvironmental indicators.

Geological setting and sample collections

The Otadai Formation in the Kazusa Group consists of alternations of turbidite sandstone and hemipelagic siltstone beds which had developed as deep-sea submarine fan systems from 1.2 to 1.0 Ma[13]. Frequently intercalated tuff beds in the Otadai Formation allows lateral bed-by-bed correlation of turbidite sandstone and siltstone beds[19]. Detailed oxygen isotope stratigraphy for the upper to middle Otadai Formation was established using benthic foraminifera recovered from the TR-3 core, which was confirmed by fission-track ages of zircon from key intercalated tuff beds, as well as magnetostratigraphy and biostratigraphy[20] (Fig. 2a). This chronological model was applied by correlations between TR-3 and the outcrops using comparison with key tuff beds (named O4, O4.5, O7, O11, O12, O16, and O18)[21], which were identified based on visual observations, mineral compositions, and refractive index of volcanic glass[20]. We collected samples from the outcrops exposed along the Yoro River, which correspond to MIS 33 to 29 (Supplementary Figs. 3a, 4). To investigate data variability within a single siltstone bed, six samples were taken from the siltstone bed ca. 10 cm below the O18 key tuff bed along the bedding plane and the turbidite sandstone directly beneath the siltstone bed (Supplementary Fig. 5). The O7 and O11 key tuff beds were also exposed at the Shoryuji section located 10 km east of the Yoro River section[22]. Siltstone samples were taken directly above and below the O7 and O11 key tuff beds in each section to compare the data from the same stratigraphic level (Supplementary Figs. 3b, 4). All samples for laboratory analysis were taken from the bluish-grey part exposed after removing the weathered surface coating on the outcrop.

Results and Discussion

LCAs and *n*-alkanes based proxies as paleoenvironmental indicators

C_{37}–C_{39} LCAs and odd preference C_{26}–C_{36} *n*-alkanes were detected in all samples that we analysed (Supplementary Fig. 6). The preservation of these biomarkers is probably due to the Kazusa Group never having been exposed to high temperatures or consolidation stress during burial and uplift. The paleo-maximum temperature and maximum burial depth deduced from vitrinite reflectance and consolidation tests in the Otadai Formation were < 45 °C and 7.6 MPa, respectively[23]. According to hydrous pyrolysis experiments, the LCAs and *n*-alkane based indices did not change under these conditions at laboratory time scales (~days)[9,10].

The alkenone unsaturation ratio ($U^{K'}_{37}$), average chain length (ACL) and carbon preference index (CPI) of *n*-alkanes (see Fig. 2 for each definition) from the Yoro River section ranged 0.795–0.921, 30.1–31.0, and 3.66–6.02, respectively, showing variations synchronised with the glacial and interglacial cycles from MIS 33 to 29 (Fig. 2). Alternatively, the relative compounds of total organic carbon and total nitrogen (C/N ratios), indicating relative contributions of terrestrial and marine organic matter (see Methods for the detail), were not completely synchronised with the glacial-interglacial cycles, suggesting that the accumulation process of organic compounds was controlled not only by sea-level changes but also by the effects of topography and redeposition in submarine fans (Fig. 2). $U^{K'}_{37}$, ACL, and CPI values from the Shoryuji section coincided with the values from the correlative siltstone bed of the Yoro River section within the data variability (2σ) of the single siltstone bed shown in Supplementary Table 1, which confirms that these indexes immune from the effects of topography in the submarine fan and faithfully reflect the representative environment around the Kazusa forearc basin (Table 1). The turbidite sandstone and the adjacent siltstones had closely similar $U^{K'}_{37}$ and ACL values

(Supplementary Table 1), which indicates that these values changed negligibly due to alternations of redox condition caused by turbidites, as is partly suggested by ref. 24. In contrast, the turbidite sand bed, which might have been redeposited from a shallower seabed[19], had a significantly higher C/N ratio and lower CPI value than the siltstones (Supplementary Table 1).

$U_{37}^{K'}$ must reflect the temperature fluctuation in the Kazusa forearc basin at water depths of 0–50 m, where LCAs are mostly produced[25]. The transportation routes of *n*-alkanes are enigmatic because they can be supplied not only as river suspensions but also as aeolian dust[26]. However, we believe that ACL and CPI fluctuations mostly reflect monsoonal climate changes in the hinterland of the Kazusa forearc basin because higher ACL and lower CPI values have been detected in the lower latitudes of present-day surface soils in East Asia as well as of aerosols in the western Pacific[27-29]. CPI values weakly correlate with C/N ratios ($R^2 = 0.31$, $p < 0.01$), whereas $U_{37}^{K'}$ and ACL do not (Supplementary Fig. 7). Therefore, CPI may also be influenced by the freshness of higher plant *n*-alkanes, that is, it declined through dilution and degradation of terrestrial plant derived material during offshore transportation and redeposition processes[6,30]. Based on the above observations, we conclude that $U_{37}^{K'}$ and ACL are less susceptible to the effects of sedimentation process and diagenesis, which can be excellent paleoenvironmental indicators for the Kazusa forearc basin. The periods and amplitudes of the terrestrial climate fluctuations indicated by ACL were almost synchronised with those of the oxygen isotope ratios of benthic foraminifera ($\delta^{18}O_{BF}$) (Fig. 2a, c). $U_{37}^{K'}$ values in the moderate interglacial periods (MIS 29 and 33) were comparable with those in the extreme interglacial period (MIS31) (Fig. 2a, b). The reason for the difference in the fluctuation pattern of $U_{37}^{K'}$ and those of ACL and $\delta^{18}O_{BF}$ can be attributed to the effect of ocean currents, as discussed in the next section.

Quantitative temperature reconstructions and implications for paleoceanography

We calculated the $U^{K'}_{37}$-SST using the global core-top calibration[3], which is largely consistent with the culture calibration of the modern alkenone synthesiser[2]. The temperature calibration may be affected by changes in the assemblages of the alkenone synthesisers, but the evolutionary events and changes in species dominance within the coccolithophore populations are considered to have had little impact on the relationship between $U^{K'}_{37}$ and SST during the Pleistocene[31,32]. The $U^{K'}_{37}$-SSTs during MIS 33 to 29 were calculated from 22.8 °C to 26.6 °C. Fluctuations in the $U^{K'}_{37}$-SST near the Boso Peninsula have been previously reported from the core site of MD01-2421 covering MIS 1–5e[33] (Fig. 1). Comparing periods with similar ice volumes estimated from the global $\delta^{18}O_{BF}$ profile[34,35], the $U^{K'}_{37}$-SSTs in the Otadai Formation appeared to be 4–7 °C higher than those of the MD01-2421 core, located near the KEF (Table 2). The ratio of magnesium to calcium (Mg/Ca) of planktic foraminifera is an additional established paleotemperature proxy[36]. From the five selected beds with relatively large amounts of foraminiferal standing stock, we analysed Mg/Ca paleotemperatures of *Globigerina bulloides* (T_{bul}), which were abundant at depths shallower than 40 m near the Boso Peninsula[37]. T_{bul} showed 19.9–21.9 °C and 22.5–24.8 °C in the glacial and interglacial periods, respectively, and these values are at least 4 °C higher than the T_{bul} from the MD01-2421 core[38], thereby supporting the validity of the high $U^{K'}_{37}$-SST (Table 2). The 1–4 °C offsets between the $U^{K'}_{37}$-SST and T_{bul} can be attributed to differences in the production seasons near the Boso Peninsula, insofar as alkenones are mostly produced in July[25], whereas *G. bulloides* are most abundant during the spring phytoplankton bloom[39]. Although these temperature offsets do not seem to be constant, similar trends can be often seen in previous studies using marine sedimentary cores[40,41], which is

161 due to that the high production season for *G. bulloides* can differ because their production is
162 greatly influenced by nutrient availability[42].

163 The $U^{K'}_{37}$-SSTs in the Otadai Formation are still 2–3 °C higher than those reported from
164 the St. 14 core covering MIS 1–2, located near the mainstream of the KC[43] (Fig. 1a, Table 2) .
165 Considering the distribution of SSTs around the core sites of MD01-2421 and St. 14
166 (Supplementary Fig. 1), we interpret that the Kazusa forearc basin was located under the direct
167 influence of the KC, and the temperatures of the warm water masses in the interglacial periods
168 (MIS 29, 31, and 33) may have been higher than those in the Holocene (MIS 1). We also
169 assumed that the KC could still have had a large influence on the Kazusa forearc basin even in
170 the glacial periods (MIS 30 and 32) compared to those in the last glacial period (MIS 2) when the
171 KEF had shifted to the south[43]. Previous studies using marine sediment cores have revealed 1–2
172 °C -higher SSTs in the California margin and eastern equatorial Pacific from 1.1 to 1.0 Ma
173 compared to the present day, while SSTs in the western equatorial Pacific have remained nearly
174 the same[44,45]. Our study, the documentation of quantitative SSTs record near the KEF, has
175 revealed that the latitudinal temperature gradient in the north-western Pacific was small,
176 indicating the widespread WPWP from 1.1 to 1.0 Ma. Changes in SST distributions during the
177 Pleistocene are important because they are considered to be linked to the mid-Pleistocene
178 transition[44]. Applying the biomarker-based proxies, the Kazusa Group can provide a long,
179 continuous, and high-time resolution paleotemperature record in the Kuroshio region, which is
180 integral to understanding Pleistocene climate changes.
181

Methods

Biomarkers and organic compounds analysis

Samples for biomarker analysis were freeze-dried after the surface was ultrasonically cleaned with ethanol and ground into a fine powder. Sediment samples were dried and crushed into a fine powder for organic matter analysis. The lipids contained in the powdered sediment (approximately 3 g) of each sample were extracted by sonication with dichloromethane/methanol (70:30, v/v) and then saponified with 0.5 mol L_1 KOH in MeOH. The saponified sample was then extracted with n-hexane to obtain the neutral components. The neutral lipids were separated into four subfractions by silica gel column chromatography. The N-1 fraction (hydrocarbons) was extracted with n-hexane/dichloromethane (95:5, v/v), and the N-2 fraction (ketones, esters, and aldehydes) was collected with n-hexane/dichloromethane (4:6, v/v). Then, they were introduced into a gas chromatograph with a mass-selective detector (GC-MS) and with a flame ionization detector (GC-FID) equipped with a VF-5ms fused silica capillary column (30 m*0.25 mm internal diameter, Agilent). The oven temperature was programmed as follows: maintained at 40 °C for 2 min, raised to 120 °C at 30 °C/min, raised to 300 °C at 6 °C/min, and maintained at 300 °C for 20 min. Several procedural blanks, which were analyzed parallelly to the same analysis, showed no C_{37} alkenone contamination. Analytical precisions (1σ) for $U^{K'}_{37}$, ACL, and CPI were 0.002, 0.008, and 0.004 units, respectively. The powdered samples used for biomarker analysis were also used for total organic carbon (TOC) and total nitrogen (TN) analysis using a Flash 2000 CHNS elemental analyser. A powdered sample (approximately 30 mg) was placed in a silver sample boat and decalcified with a few drops of 1 N HCl and then dried for at least 2 hr at 80 °C to remove unreacted HCl and water. The dried samples were wrapped in a tin sample boat for combustion. Quantification errors for TOC and TN were both 3 % (1σ) based on

replicated analyses of a 2,5-bis-(5-tertbutyl-benzoxazol-2-yl)-thiophene standard. In this study, C/N ratios were used to clarify the source of organic matter, as the C/N ratio of typical marine phytoplankton organic matter is 6–7, whereas that of terrestrial organic matter is > 12 due to the contribution of lignin-phenols[46].

Mg/Ca ratios analysis

Mg/Ca ratios of the planktic foraminifera *G. bulloides* were analysed for five selected siltstone beds with relatively large amounts of foraminiferal standing stock and good preservation to reproduce the surface temperature. Samples for handpicking fossil foraminifera were disaggregated using Na_2SO_4. Mg/Ca ratios were measured using *G. bulloides* from the > 210 μm size fraction. Ten or more white individuals without an oxide film were used for the measurements. The samples were cleaned using the following methods outlined by ref. 47. We modified the methods for the foraminiferal tests following ref. 48. Initially, the samples were gently crushed into fragments and then rinsed with methanol and ultrapure water. This process was repeated until all loose material (i.e., nannofossils and clay) was removed. The samples were then treated with an oxidising agent that consisted of H_2O_2 and KOH to remove organic matter. Finally, the samples were rinsed with a mixture of H_2O_2 and $HClO_4$. Mg, Ca, and Mn concentrations were obtained by inductively coupled plasma mass spectrometry (ICP-MS). For ICP-MS analysis, a powdered carbonate sample was transferred to Teflon vials, and 0.3 M HNO_3 was added to each vial to dissolve the solids. The HNO_3 used in this study was a commercially supplied high-purity TAMAPURE AA-100 reagent (Tama Chemical, Japan). To control the instrumental drift, internal standards (Be, Sc, Y, and I) were added to HNO_3. Additionally, standard solutions prepared from JCp-1 (Geological Survey of Japan)[49] were measured for use in

data correction. The relative standard deviation based on replicate measurements of JCp-1 was 0.5 % (1σ). The Mn/Ca ratios were 0.5 mmol/mol or less for all measured samples, indicating that the precleaning was sufficiently performed[50]. The Mg/Ca ratios of *G. bulloides* were converted to a temperature scale using the calibration in ref. 51.

Acknowledgements

We would appreciate Y. Ota, Y. Isaji, S. Furota, H. Suga, N.O. Ogawa, Y. Takano, K.M. Matsuzaki and Y. Nishikura for their helpful advice and assistance in the laboratory work. T. Tsuji provided information about the TR-3 core. This research was partly supported by a Grant-in-Aid from the Japan Society for the Promotion of Science (18J21788) given to H. Kajita.

Author contributions

H. Kajita and M.U designed the project and conducted the field survey. H. Kajita and A.M analyzed the samples. T.Y, N.O, A.S, and H. Kawahata organized the laboratory work and assisted data interpretations. H. Kajita wrote the manuscript. All authors contributed to editing and revision.

Competing interests

The authors declare no competing interests.

References

1. Marlowe, I. T. *et al*. Long chain (n-C_{37}–C_{39}) alkenones in the Prymnesiophyceae. Distribution of alkenones and other lipids and their taxonomic significance. *Br. Phycol. J.* **19,** 203-216 (1984).
2. Prahl, F. G., Muehlhausen, L. A. & Zahnle, D. L. Further evaluation of long-chain alkenones as indicators of paleoceanographic conditions. *Geochim. Cosmochim. Acta* **52**, 2303-2310 (1988).
3. Müller, P. J., Kirst, G., Ruhland, G., Von Storch, I. & Rosell-Melé, A. Calibration of the alkenone paleotemperature index $U_{37}^{K'}$ based on core-tops from the eastern South Atlantic and the global ocean (60° N-60° S). *Geochim. Cosmochim. Acta* **62,** 1757-1772 (1998).
4. Conte, M. H., Thompson, A., Lesley, D. & Harris, R. P. Genetic and physiological influences on the alkenone/alkenoate versus growth temperature relationship in *Emiliania huxleyi* and *Gephyrocapsa oceanica*. *Geochim. Cosmochim. Acta* **62,** 51-68 (1998).
5. Eglinton, G. & Hamilton, R. J. The distribution of alkanes. In *Chemical plant Taxonomy* (Elsevier B.V., Amsterdam, 1963).
6. Rielley, G., Collier, R. J., Jones, D. M. & Eglinton, G. The biogeochemistry of Ellesmere Lake, UK–I: source correlation of leaf wax inputs to the sedimentary lipid record. *Org. Geochem.* **17,** 901-912 (1991).
7. Baczynski, A. A., McInerney, F. A., Freeman, K. H., Wing, S. L. & Bighorn Basin Coring Project (BBCP) Science Team. Carbon Isotope Record of Trace n-alkanes in a Continental PETM Section Recovered by the Bighorn Basin Coring Project (BBCP). *Paleoceanogr. Paleoclimatol.* **34,** 853-865 (2019).
8. Sawada, K., Ono, M., Nakamura, H. & Tareq, S. M. Reconstruction of Holocene Optimum

paleoclimatic variations using long-chain n-alkanes and alkenones in sediments from Dabusu Lake, northeastern China. *Quat. Int.* **550,** 27-38 (2020).

9. Rabinowitz, H. S., Polissar, P. J. & Savage, H. M. Reaction kinetics of alkenone and n-alkane thermal alteration at seismic timescales. *Geochemistry, Geophys. Geosystems* **18,** 204-219 (2017).
10. Wang, C., Eley, Y., Oakes, A. & Hren, M. Hydrogen isotope and molecular alteration of n-alkanes during heating in open and closed systems. *Org. Geochem.* **112,** 47-58 (2017).
11. Cleaveland, L. C. & Herbert, T. D. Preservation of the alkenone paleotemperature proxy in uplifted marine sequences: A test from the Vrica outcrop, Crotone, Italy. *Geology* **37**, 179-182 (2009).
12. Herbert, T. D., Ng, G. & Peterson, L. C. Evolution of Mediterranean sea surface temperatures 3.5–1.5 Ma: regional and hemispheric influences. *Earth planet. Sci. Lett.* **409,** 307-318 (2015).
13. Ito, M. & Katsura, Y. Inferred glacio-eustatic control for high-frequency depositional sequences of the Plio-Pleistocene Kazusa Group, a forearc basin fill in Boso Peninsula, Japan. *Sediment. Geol.* **80,** 67-75 (1992).
14. Kazaoka, O. *et al*. Stratigraphy of the Kazusa Group, Boso Peninsula: An expanded and highly-resolved marine sedimentary record from the Lower and Middle Pleistocene of central Japan. *Quat. Int.* **383,** 116-135 (2015).
15. Suganuma, Y. *et al*. (2018). Paleoclimatic and paleoceanographic records through Marine Isotope Stage 19 at the Chiba composite section, central Japan: A key reference for the Early–Middle Pleistocene Subseries boundary. *Quat. Sci. Rev.* **191,** 406-430.
16. Gradstein, F. M., Ogg, J. G., Schmitz, M. B. & Ogg, G. M. *Geologic Time Scale 2020, Second*

294 *Edition* (Elsevier B.V., Amsterdam, 2020).
295 17. Kida, S. *et al*. Oceanic fronts and jets around Japan: a review. In *"Hot Spots" in the Climate*
296 *System* (Springer, Tokyo, 2016).
297 18. Tada, R., Zheng, H. & Clift, P. D. Evolution and variability of the Asian monsoon and its
298 potential linkage with uplift of the Himalaya and Tibetan Plateau. *Prog. Earth Planet. Sci.* **3,**
299 4 (2016).
300 19. Hirayama, J. & Nakajima, T. Analytical study of turbidites, Otadai Formation, Boso Peninsula,
301 Japan. *Sedimentology* **24,** 747-779 (1977).
302 20. Tsuji, T. *et al*. High-resolution chronology of the lower Pleistocene Otadai and Umegase
303 Formations of the Kazusa Group, Boso Peninsula, central Japan – Chronostratigraphy of the
304 JNOC TR-3 cores based on oxygen isotope, magnetostratigraphy and calcareous nannofossil
305 –. *J. Geol. Soc. Japan* **111,** 1-20 (2005).
306 21. Nanayama, F., Nakazato, H., Ooi, S. & Nakashima, R. *Geology of the Mobara Distinct.*
307 *Quadrangle Series, 1:50,000* (Geological Survey of Japan, AIST, Tsukuba, 2016).
308 22. Utsunomiya, M. & Ooi, S. *Geology of the Kazusa-Ohara Distinct. Quadrangle Series,*
309 *1:50,000* (Geological Survey of Japan, AIST, Tsukuba, 2019).
310 23. Kamiya, N. *et al*. Major variations in vitrinite reflectance and consolidation characteristics
311 within a post-middle Miocene forearc basin, central Japan: A geodynamical implication for
312 basin evolution. *Tectonophysics* **710,** 69-80 (2017).
313 24. Prahl, F. G., De Lange, G. J., Lyle, M. & Sparrow, M. A. Post-depositional stability of long-
314 chain alkenones under contrasting redox conditions. *Nature* **341,** 434-437 (1989).
315 25. Sawada, K., Handa, N. & Nakatsuka, T. Production and transport of long-chain alkenones and
316 alkyl alkenoates in a sea water column in the northwestern Pacific off central Japan. *Mar.*

317 *Chem.* **59,** 219-234 (1998).
318 26. Ohkouchi, N., Kawamura, K., Kawahata, H. & Taira, A. Latitudinal distributions of terrestrial
319 biomarkers in the sediments from the Central Pacific. *Geochim. Cosmochim. Acta* **61,** 1911-
320 1918 (1997).
321 27. Bendle, J., Kawamura, K., Yamazaki, K. & Niwai, T. Latitudinal distribution of terrestrial lipid
322 biomarkers and n-alkane compound-specific stable carbon isotope ratios in the atmosphere
323 over the western Pacific and Southern Ocean. *Geochim. Cosmochim. Acta* **71,** 5934-5955
324 (2007).
325 28. Rao, Z. *et al*. Compound specific δD values of long chain n-alkanes derived from terrestrial
326 higher plants are indicative of the δD of meteoric waters: Evidence from surface soils in
327 eastern China. *Org. Geochem.* **40,** 922-930 (2009).
328 29. Luo, P., Peng, P., Lü, H., Zheng, Z. & Wang, X. Latitudinal variations of CPI values of long-
329 chain n-alkanes in surface soils: Evidence for CPI as a proxy of aridity. *Sci. China Earth Sci.*
330 **55,** 1134-1146 (2012).
331 30. Zhang, J., Yu, H., Jia, G., Chen, F. & Liu, Z. Terrestrial n-alkane signatures in the middle
332 Okinawa Trough during the post-glacial transgression: control by sea level and
333 paleovegetation confounded by offshore transport. *Geo-Mar. Lett.* **30,** 143-150 (2010).
334 31. Müller, P. J., Čepek, M., Ruhland, G. & Schneider, R. R. Alkenone and coccolithophorid
335 species changes in late Quaternary sediments from the Walvis Ridge: Implications for the
336 alkenone paleotemperature method. *Palaeogeogr. Palaeoclimatol. Palaeoecol.* **135,** 71-96
337 (1997).
338 32. McClymont, E. L., Rosell-Melé, A., Giraudeau, J., Pierre, C. & Lloyd, J. M. Alkenone and
339 coccolith records of the mid-Pleistocene in the south-east Atlantic: Implications for the $U_{37}^{K'}$

index and South African climate. *Quat. Sci. Rev.* **24,** 1559-1572 (2005).

33. Lisiecki, L. E. & Raymo, M. E. A Pliocene-Pleistocene stack of 57 globally distributed benthic $\delta^{18}O$ records. *Paleoceanography* **20,** PA1003 (2005).
34. Elderfield, H., Ferretti, P., Greaves, M., Crowhurst, S., McCave, I. N., Hodell, D., & Piotrowski, A. M. Evolution of ocean temperature and ice volume through the mid-Pleistocene climate transition. *Science* **337**, 704-709 (2012).
35. Yamamoto, M., Oba, T., Shimamune, J. & Ueshima, T. Orbital-scale anti-phase variation of sea surface temperature in mid-latitude North Pacific margins during the last 145,000 years. *Geophys. Res. Lett.* **31,** L16311 (2004).
36. Nürnberg, D., Bijma, J. & Hemleben, C. Assessing the reliability of magnesium in foraminiferal calcite as a proxy for water mass temperatures. *Geochim. Cosmochim. Acta* **60,** 803-814 (1996).
37. Kuroyanagi, A. & Kawahata, H. Vertical distribution of living planktonic foraminifera in the seas around Japan. *Mar. Micropaleontol.* **53,** 173-196 (2004).
38. Oba, T. & Murayama, M. Sea-surface temperature and salinity changes in the northwest Pacific since the Last Glacial Maximum. *J. Quat. Sci.* **19,** 335-346 (2004).
39. Oda, M. & Yamasaki, M. Sediment trap results from the Japan Trench in the Kuroshio domain: seasonal variations in the planktic foraminiferal flux. *J. Foraminiferal Res.* **35,** 315-326 (2005).
40. Nürnberg, D., Müller, A. & Schneider, R. R. Paleo-sea surface temperature calculations in the equatorial east Atlantic from Mg/Ca ratios in planktic foraminifera: A comparison to sea surface temperature estimates from $U^{K'}_{37}$, oxygen isotopes, and foraminiferal transfer function. *Paleoceanography* **15,** 124-134 (2000).
41. Bard, E. Comparison of alkenone estimates with other paleotemperature proxies.

Geochemistry, Geophys. Geosystems **2,** 2000GC000050 (2001).

42. Kuroyanagi, A., Kawahata, H., Nishi, H. & Honda, M. C. Seasonal to interannual changes in planktonic foraminiferal assemblages in the northwestern North Pacific: Sediment trap results encompassing a warm period related to El Niño. *Palaeogeogr. Palaeoclimatol. Palaeoecol.* **262,** 107-127 (2008).
43. Sawada, K. & Handa, N. Variability of the path of the Kuroshio ocean current over the past 25,000 years. *Nature* **392,** 592-595 (1998).
44. McClymont, E. L., Sosdian, S. M., Rosell-Melé, A. & Rosenthal, Y. Pleistocene sea-surface temperature evolution: Early cooling, delayed glacial intensification, and implications for the mid-Pleistocene climate transition. *Earth Sci. Rev.* **123,** 173-193 (2013).
45. Fedorov, A. V., Burls, N. J., Lawrence, K. T. & Peterson, L. C. Tightly linked zonal and meridional sea surface temperature gradients over the past five million years. *Nat. Geosci.* **8,** 975-980 (2015).
46. Lamb, A. L., Vane, C. H., Wilson, G. P., Rees, J. G. & Moss-Hayes, V. L. Assessing $\delta^{13}C$ and C/N ratios from organic material in archived cores as Holocene sea level and palaeoenvironmental indicators in the Humber Estuary, UK. *Mar. Geol.* **244,** 109-128 (2007).
47. Cheng, H., Adkins, J., Edwards, R. L. & Boyle, E. A. U-Th dating of deep-sea corals. *Geochim. Cosmochim. Acta* **64,** 2401-2416 (2000).
48. Yoshimura, T. *et al*. Altervalent substitution of sodium for calcium in biogenic calcite and aragonite. *Geochim. Cosmochim. Acta* **202,** 21-38 (2017).
49. Okai, T. Collaborative analysis of GSJ/AIST geochemical reference materials JCp-1 (Coral) and JCt-1 (Giant Clam). *Geochemistry (Chikyukagaku)* **38,** 281-286 (2004).
50. Hasenfratz, A. P. *et al*. Determination of the Mg/Mn ratio in foraminiferal coatings: An

approach to correct Mg/Ca temperatures for Mn-rich contaminant phases. *Earth planet. Sci. Lett.* **457,** 335-347 (2017).

51. Mashiotta, T. A., Lea, D. W. & Spero, H. J. Glacial–interglacial changes in Subantarctic sea surface temperature and δ^{18}O-water using foraminiferal Mg. *Earth Planet. Sci. Lett.* **170,** 417-432 (1999).

Figure legends

Figure 1. Maps showing overall setting of the Kazusa Group in central Japan. (a) Bold yellow arrow and green dotted line represent the general path of the KC and KEF in the present day, respectively. The bathymetry, plate boundaries, and locations of cores MD01-2421 and St. 14 (red squares) are also shown. (b) Surface distribution of the Otadai formation (yellow-coloured) in the Kazusa Group (grey-coloured) on the Boso Peninsula, showing the locations of survey sites in this study (red triangles) and TR-3 core (open square).

Figure 2. Biomarker profiles in the Yoro River section. (a) Oxygen isotope stratigraphy of the TR-3 core, which is comparable to the Yoro River section[20]. Triangles show age-control horizons established by correlation with deep sea core ODP site 677. The base of Jaramillo normal subchronozone is shown with the shaded area. The intercalated key tuff beds are shown with dotted lines, one of which (O7) was dated by zircon fission track (1.0 ± 0.2 Ma). (b) $U^{K'}_{37}$ (=$\{C_{37:2}\}/\{C_{37:2}\}+\{C_{37:3}\}$), (c) ACL (=$\Sigma x[C_x]/[C_x]$), (d) CPI (=$2*\Sigma[C_x]/(\Sigma[C_y]+\Sigma[C_z])$), and (e) C/N ratios, where { } and [] represents concentrations of each carbon number of LCAs and *n*-alkanes, respectively (x = 27, 29, 31, 33, 35; y = 26, 28, 30, 32, 34; z = 28, 30, 32, 34, 36). Grey lines connect the strata from which samples for biomarker analysis were not collected because of the far distance from the key tuff beds. The error bars indicate the standard deviations based on six samples taken from the siltstone bed (S-29-1–6) (Supplementary Table 1). Detailed information on the sampling locations is shown in Supplementary Figure 4 and Supplementary Table 2.

414 **Tables**

415 Table 1. Comparison of multiple proxy records in strata at the same level in the Yoro River and

416 Shoryuji sections.

417

	Section	Sample ID	$U^{K'}_{37}$	$U^{K'}_{37}$-SST (°C)	ACL	CPI	C/N
Directly above the O7 key tuff bed	Yoro River	S-26	0.849	24.4	30.6	5.69	6.8
	Shoryuji	S-18	0.869	25.0	30.5	5.44	6.4
Directly below the O7 key tuff bed	Yoro River	Y-05	0.827	23.7	30.6	5.66	10.4
	Shoryuji	S-19	0.830	23.8	30.5	4.92	8.4
Directly above the O11 key tuff bed	Yoro River	S-42	0.919	26.5	30.6	4.00	6.9
	Shoryuji	S-17	0.912	26.3	30.5	4.35	7.4
Directly below the O11 key tuff bed	Yoro River	Y-03	0.873	25.1	31.0	4.40	8.9
	Shoryuji	S-16	0.886	25.5	30.8	4.04	7.7

418

419 Table 2. Paleotemperatures estimated from $U^{K'}_{37}$ and Mg/Ca ratios of *Globigerina bulloides* in the

420 Otadai Formation. Data from core MD01-2421[35,38] and St. 14[43] are also shown.

421

Location	Sample ID	MIS	$U^{K'}_{37}$-SST (°C) (Alkenone)	Mg/Ca-SST (°C) (*G. bulloides*)
Otadai F.	S-29	33	26.1	23.3
Otadai F.	S-32	33	26.5	22.5
Otadai F.	S-24	32	23.6	21.9
Otadai F.	S-10	31	25.7	24.8
Otadai F.	S-26	30	24.3	19.9
MD01-2421		5e	ca. 20－23	-
MD01-2421		5a–d	ca. 19－21	
MD01-2421		4	ca. 18	-
MD01-2421		3	ca. 17－19	-
MD01-2421		2	ca. 13－16	ca. 7－8
MD01-2421		1	ca. 17－21	ca. 16－18
St.14		2	ca. 20－22	-
St.14		1	ca. 22－24	-

422

423

424 **Figures**

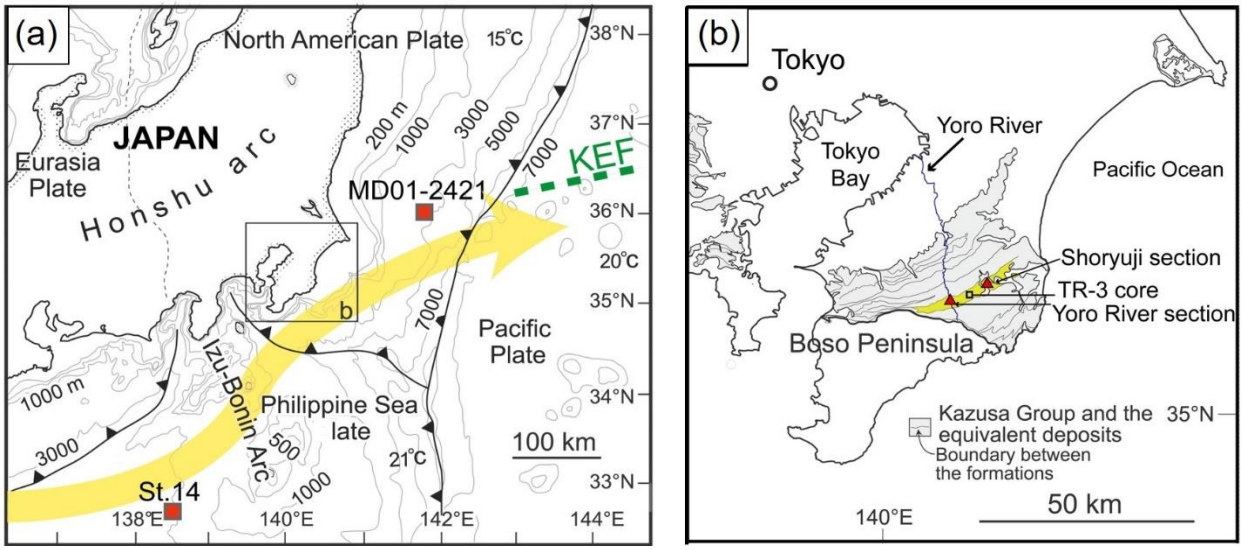

425

426 Figure. 1

427

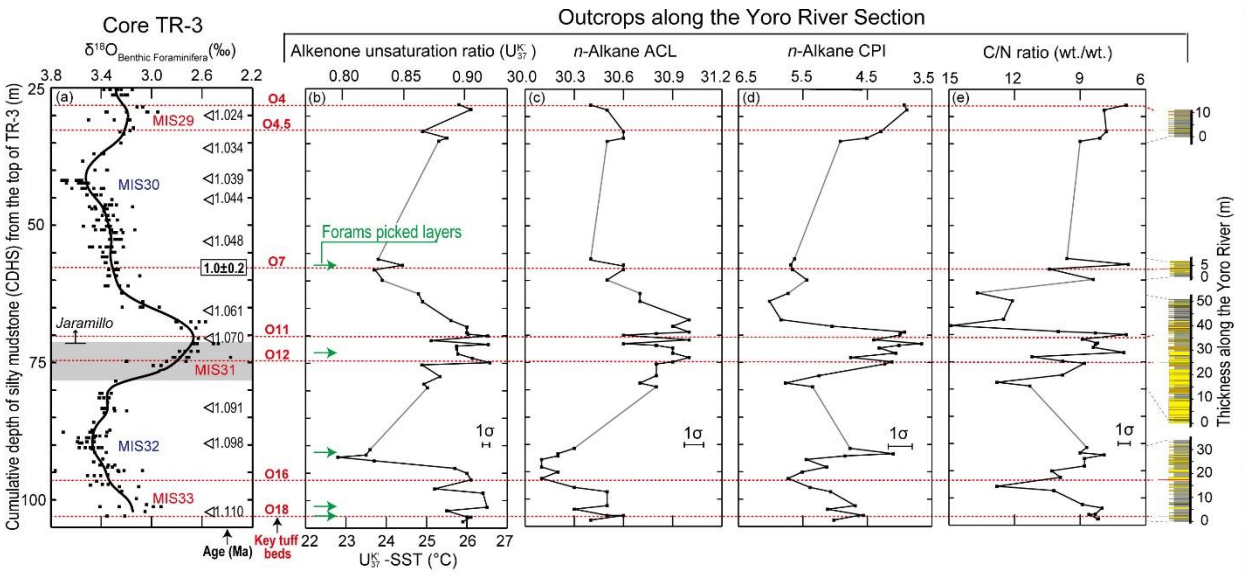

428

429 Figure. 2

Figures

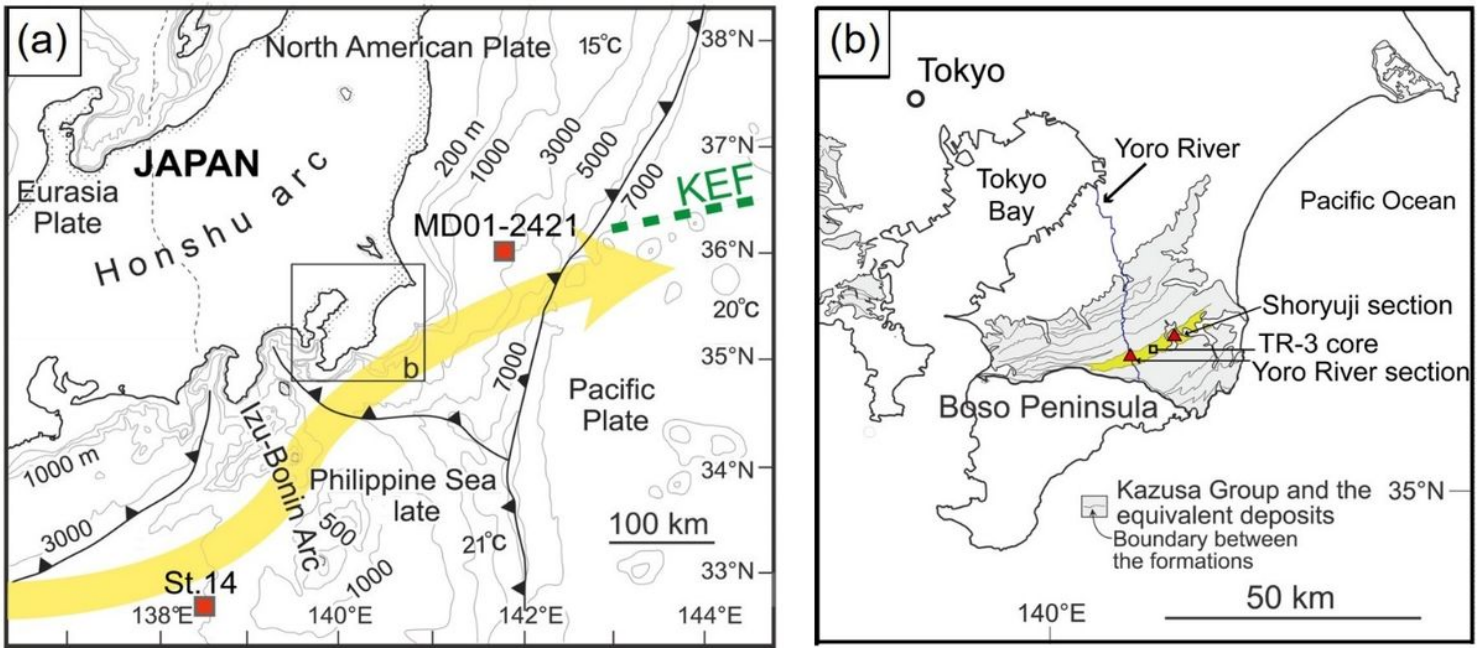

Figure 1

Maps showing overall setting of the Kazusa Group in central Japan. (a) Bold yellow arrow and green dotted line represent the general path of the KC and KEF in the present day, respectively. The bathymetry, plate boundaries, and locations of cores MD01-2421 and St. 14 (red squares) are also shown. (b) Surface distribution of the Otadai formation (yellow-coloured) in the Kazusa Group (grey-coloured) on the Boso Peninsula, showing the locations of survey sites in this study (red triangles) and TR-3 core (open square).

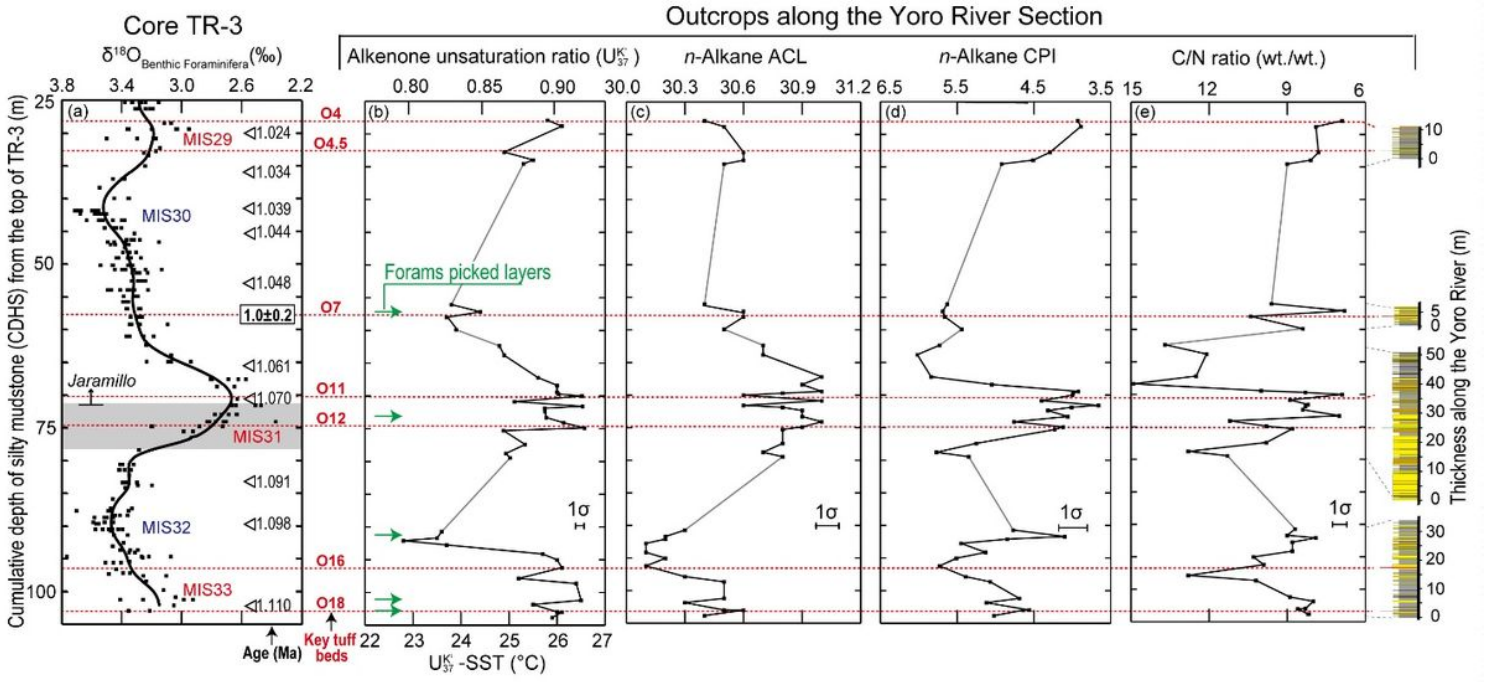

Figure 2

Biomarker profiles in the Yoro River section. (a) Oxygen isotope stratigraphy of the TR-3 core, which is comparable to the Yoro River section20. Triangles show age-control horizons established by correlation with deep sea core ODP site 677. The base of Jaramillo normal subchronozone is shown with the shaded area. The intercalated key tuff beds are shown with dotted lines, one of which (O7) was dated by zircon fission track (1.0 ± 0.2 Ma). (b) "U" _"37" ^"K'" (={C37:2}/{C37:2}+{C37:3}), (c) ACL (=Σx[Cx]/[Cx]), (d) CPI (=2*Σ[Cx]/(Σ[Cy]+Σ[Cz])), and (e) C/N ratios, where {} and [] represents concentrations of each carbon number of LCAs and n-alkanes, respectively (x = 27, 29, 31, 33, 35; y = 26, 28, 30, 32, 34; z = 28, 30, 32, 34, 36). Grey lines connect the strata from which samples for biomarker analysis were not collected because of the far distance from the key tuff beds. The error bars indicate the standard deviations based on six samples taken from the siltstone bed (S-29-1–6) (Supplementary Table 1). Detailed information on the sampling locations is shown in Supplementary Figure 4 and Supplementary Table 2.

Supplementary Files

This is a list of supplementary files associated with this preprint. Click to download.

- SupplementaryMaterialscommEE.docx